AIAA 81-0252R

Prediction of Subsonic Aerodynamic Characteristics: A Case for Low-Order Panel Methods

Brian Maskew*
Analytical Methods, Inc., Redmond, Wash.

A low-order panel method is presented for the calculation of subsonic aerodynamic characteristics of general configurations. The method is based on piecewise constant doublet and source singularities. Two forms of the internal Dirichlet boundary condition are discussed and the source distribution is determined by the external Neumann boundary condition. Calculations are compared with higher-order solutions for a number of cases. It is demonstrated that for comparable density of control points where the boundary conditions are satisfied, the low-order method gives comparable accuracy to the higher-order solutions. It is also shown that problems associated with some earlier low-order panel methods, e.g., leakage in internal flows and junctions and also poor trailing-edge solutions, do not appear for the present method. Further, the application of the Kutta condition is extremely simple; no extra equation or trailing-edge velocity point is required. The method has very low computing costs and this has made it practical for application to nonlinear problems requiring iterative solutions and to three-dimensional unsteady problems using a time-stepping approach. In addition, the method has been extended to model separated flows in three dimensions, using free vortex sheets to enclose the separated zone.

Nomenclature

C_p	= pressure coefficient
C_L	= lift coefficient
C_D	= drag coefficient
n	= surface unit normal vector directed into the flowfield
N	= number of panels
S	= surface of configuration; i.e., wing, body, etc.
t	= surface tangent vector
V	= velocity
W	= wake surface
x,y,z	= Cartesian coordinates in a body fixed frame
α	= onset flow incidence to the body x axis
Γ	= circulation value
μ	= doublet strength
σ	= source strength
Φ	= total velocity potential
ϕ	= perturbation velocity potential
∇	= gradient operator

Subscripts

JK	= values on panels J, K, respectively
L	= lower
i	= interior
P	= point
S	= surface of wing, body, etc.
U	= upper
W	= wake
∞	= reference onset condition

Introduction

ALTHOUGH remarkable advances are being made in flowfield calculations using finite-difference and also finite-element methods, the surface integral approach of panel methods coupled with corrections for compressibility and viscous effects still offers distinct advantages for subcritical (e.g., Refs. 1-3) and also supersonic analysis (e.g., Ref. 4). In particular, panel methods offer greater versatility for practical applications to complicated configurations and are considerably more efficient in terms of computing effort. Moreover, the concept of zonal modeling (e.g., Ref. 5), in which a local field calculation is coupled with a panel method analysis, looks attractive for extending the practical scope of panel methods into the transonic regime.

The present paper discusses a general low-order panel method for predicting subsonic aerodynamic characteristics of complex configurations. It is based on piecewise constant surface singularity distributions. The method has evolved over a number of years with the overall objective being a practical engineering tool having low computing costs.

Over the past decade, panel methods have seen a trend towards higher-order formulation (e.g., Refs. 6-9). At the outset it was argued that compared with the earlier low-order methods, the more continuous representation of the surface singularity distribution should allow a reduction in panel density for a given solution accuracy, and hence should lead to lower computing costs. No such benefits have appeared so far for the general three-dimensional case. In the meantime, further developments of piecewise constant singularity panel methods, e.g., Morino[10] and the method described in this paper, are giving comparable accuracy at even lower computing costs.

The simplicity of piecewise constant singularity panels offers great flexibility for application to general problems; since continuity of singularity distribution is not enforced from panel to panel the assembly of panels representing a complicated surface is fairly straightforward. The method has been successfully applied to complete aircraft configurations (not yet reported) involving high-lift devices, powered engine nacelles, flap-track fairings, etc. The low computing cost makes it practical to apply the method to nonlinear problems requiring iterative solutions, e.g., wake-relaxation for high-lift and/or multiple component problems; viscous/inviscid calculations with coupled boundary layer codes, including the case with extensive separation[11]; and also time-stepping calculations for three-dimensional unsteady problems.[12,13]

An outline of the method and discussion of the boundary conditions follow a brief comparison of high-order vs low-order formulations for the numerical solution of a vortex/surface interaction. Various applications of the method to three-dimensional problems are then discussed; some of the cases are compared with higher-order solutions and others with experimental results. Computing *costs* as well as CPU times are discussed. Most computing systems now include an

Presented as Paper 81-0252 at the AIAA 19th Aerospace Sciences Meeting, St. Louis, Mo., Jan. 12-15, 1981; submitted March 4, 1981; revision received July 6, 1981.

*Vice President, Research. Member AIAA.

input/output data transfer term in the cost algorithm; this severely penalizes higher-order codes which require a large amount of disk storage for the high-order interpolation data.

Basic Considerations

Calculations involving close interaction regions, e.g., surface/wake, junction flows and internal flows, behaved badly with earlier low-order panel methods. Higher-order formulations should certainly solve these problems and have been pursued in the past (e.g., Ref. 7), but, care is needed in the choice of interpolation function; a piecewise higher-order representation can "flavor" the solution unless it matches the actual form of the local distribution. Over most of the surface of an aircraft configuration, second- or third-order polynomials can match the singularity distribution adequately when given a reasonable panel density, but this is not the case in regions of high curvature such as near the wing leading edge or tip edge, in junctions, and also in the close interaction region between a vortex and a surface. For example, the latter case has been examined in isolation using the two-dimensional problem of a vortex above a plane. The exact solution for the doublet distribution on the plane such that the latter is a streamline of the flow is

$$\mu(x) = (-\Gamma/\pi)\tan^{-1}(x/h) \qquad (1)$$

where x is measured along the plane from a point directly below the vortex and h is the height of the vortex above the plane. The exact velocity distribution on the plane is

$$V(x) = -\frac{d\mu}{dx} = \frac{\Gamma}{\pi}\frac{h}{x^2+h^2}$$

This is plotted in Fig. 1.

A piecewise quadratic doublet distribution has difficulty in representing the arctangent function in Eq. (1); consequently, a panel method based on such a model may require a high density of control points (where the boundary condition of zero normal velocity is applied) in order to achieve good accuracy (Fig. 1). The local panel density required would depend on the vortex height above the surface. In fact, for meaningful results the distance between control points should be less than the height of the vortex above the surface.

Results from a piecewise constant doublet model are included in Fig. 1 for comparison and it is interesting to observe that with the same density of control points the simple model gives almost the same accuracy as in the higher-order case. (Both models solve for the doublet value at each panel center, and the velocity value $-d\mu/dx$ is evaluated by central differencing here.) Note that in the 120-panel case the two solutions are essentially identical.

The main point to be made here is that in a close interaction situation the main factor affecting the solution accuracy appears to be the density of control points—the order of the singularity distribution has only a small influence. (Obviously, this statement is based on using a reasonably convenient higher-order function, e.g., polynomial. Clearly, in the present case a higher-order formulation based on Eq. (1) would require fewer boundary condition equations, but the influence coefficient expression would be very cumbersome for the general case.)

The calculation of the vortex/surface interaction problem is considered further in Ref. 14 where it is demonstrated that the calculation can be made nominally exact by the use of a simple subpanel technique. The technique also allows off-body velocity calculations to be made at arbitrary points near the surface even with low-order paneling.[15]

The piecewise constant doublet model has already proven to be a versatile tool in both the horseshoe vortex-lattice and quadrilateral vortex-lattice methods (e.g., Ref. 16). The quadrilateral vortex form[12,17] is particularly useful for high-lift and wake roll-up calculations. Application to closed

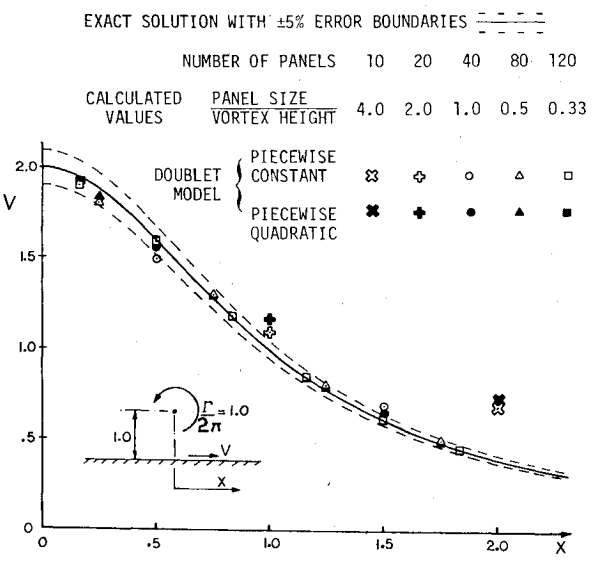

Fig. 1 Velocity distribution on a plane in the presence of a vortex.

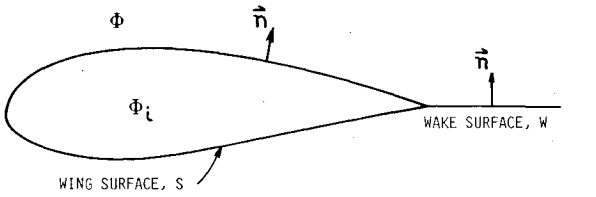

Fig. 2 Section through a wing and its wake.

surfaces were briefly examined[17] but required special treatment when using the external Neumann boundary condition; in particular, this produces ill-conditioning in the boundary condition equations near the trailing edge.[15] However, it can be shown that when a closed body is represented by a surface distribution of normal doublets and the Neumann boundary condition of zero normal velocity is applied, then the interior flow is stationary, i.e., constant velocity potential. This offers an alternative way of satisfying the exterior boundary condition and was used earlier in two-dimensional flow,[18,19] setting the internal tangential velocity to zero. This approach demonstrated good conditioning even in the case of a cusped trailing edge.

In the three-dimensional case it is more appropriate to consider the internal velocity potential directly; i.e., the interior Dirichlet boundary condition. This approach has the advantage of working with a scalar quantity rather than with the velocity vector. The fact that the velocity is the *gradient* of the potential means that the potential formulation behaves as if it is one order higher than the velocity formulation for a given order of singularity distribution. This was demonstrated numerically by Bristow.[9] A disadvantage of the Dirichlet approach is that the formulation usually results in a solution for the surface velocity potential; thus numerical differentiation is required in order to evaluate the velocity distribution. The fact that numerical differentiation can lead to inaccuracies in awkward situations has deterred many would-be users of the internal potential formulation in the past.

Internal Dirichlet Formulation

In Fig. 2 we have taken a cut through a wing and its semi-infinite wake.

We assume the existence of velocity potentials Φ in the flowfield and Φ_i inside the wing. For the present discussion we assume the wake has vanishing thickness and that it has zero entrainment. Applying Green's Theorem to the inner and outer regions and combining the resulting expressions, the

velocity potential at a point P on the inside surface can be written

$$4\pi\Phi_p = \int\int_{S-P} (\Phi-\Phi_i)\boldsymbol{n}\cdot\nabla\left(\frac{1}{r}\right)\mathrm{d}S - 2\pi(\Phi-\Phi_i)_p + \int\int_W (\Phi_U-\Phi_L)\boldsymbol{n}\cdot\nabla\left(\frac{1}{r}\right)\mathrm{d}W + \int\int_S \frac{1}{r}\boldsymbol{n}\cdot(\nabla\Phi_i-\nabla\Phi)\mathrm{d}S + 4\pi\phi_{\infty p} \quad (2)$$

where r is the length of the vector from the surface element to the point P, and $S-P$ signifies that the point P is excluded from the surface integral. Equation (2) gives the total potential at the interior point P as the sum of perturbation potentials due to a normal doublet distribution of strength ($\Phi-\Phi_i$ on S and $\Phi_U-\Phi_L$ on W, respectively) and a source distribution of strength, $\boldsymbol{n}\cdot(\nabla\Phi_i-\nabla\Phi)$ on S. The potential for a uniform onset flow, ϕ_∞, is also included.

In principle, an infinite number of combinations of doublet and source distribution will give the same external flowfield, but different internal flowfields. To render a unique combination of singularities, we can either specify one of the singularity distributions (e.g., $\sigma=0$ in the doublet-only formulation) or, as in the present case, we can specify the internal flow. Below, we consider two internal flows from a wide range of possibilities.

Zero Flow Inside

Consider first the interior stagnation condition which was implied by the earlier piecewise constant doublet codes[12,17] which used the exterior Neumann boundary condition $\boldsymbol{V}\cdot\boldsymbol{n}=0$. For the present formulation we set $\Phi_i=\text{const}=0$, say in Eq. (2), giving

$$4\pi\Phi_p = 0 = \int\int_{S-P} \Phi\boldsymbol{n}\cdot\nabla\left(\frac{1}{r}\right)\mathrm{d}S - 2\pi\Phi_p + \int\int_W (\Phi_U-\Phi_L)\boldsymbol{n}\cdot\nabla\left(\frac{1}{r}\right)\mathrm{d}W - \int\int_S \frac{1}{r}\boldsymbol{n}\cdot\nabla\Phi\mathrm{d}S + \Phi_{\infty p} \quad (3)$$

The source distribution $-\boldsymbol{n}\cdot\nabla\Phi$ is now the *total* normal velocity of the fluid at the surface S. This must satisfy the external Neumann boundary condition; i.e., the resultant normal velocity relative to the surface is

$$V_N = -\boldsymbol{n}\cdot\nabla\Phi - \boldsymbol{n}\cdot\boldsymbol{V}_S$$

where $\boldsymbol{V}_S$ is the local velocity of the surface. This may be composed of several parts due to body rotation (e.g., pitch oscillation[13] or helicopter blade rotation), translation, growth,[14] etc.

The resultant normal velocity V_N may have a nonzero value. It can be used to represent boundary-layer displacement effect by transpiration, also inflow/outflow for engine inlet/exhaust, and so on.

Thus the source distribution, in general, is given by

$$\sigma = -\boldsymbol{n}\cdot\nabla\Phi = V_N + \boldsymbol{n}\cdot\boldsymbol{V}_S \quad (4)$$

For the present discussion, we consider the case of a fixed surface with zero resultant normal velocity, hence the source term disappears from Eq. (3). Thus the basic unknown is the surface doublet distribution, which is numerically equal to the velocity potential at the surface with this formulation.

For a numerical solution of Eq. (3), we represent the surface and wake by a number of flat quadrilateral panels and we assume the singularity distribution is constant over each panel. Equation (3) is applied at a central control point on the under side of each surface panel. If there are N_S surface panels, we have N_S equations in N_S (unknown) panel doublet values.

Thus Eq. (3) becomes

$$\sum_{K=1,K\neq J}^{N_S} (\mu_K C_{JK}) - 2\pi\mu_J + \sum_{K=1}^{N_W} (\mu_{W_K} C_{JK}) = 0 \qquad J = 1, N_S \quad (5)$$

The influence coefficient C_{JK} is an arctangent function for the velocity potential induced at the control point J by a unit uniform doublet distribution on panel K.

The wake doublet values are determined by the Kutta condition and the type of problem. In the case of unsteady flows[13] and separated flow models,[11] μ_W varies in the streamwise as well as spanwise directions. Here we consider just the basic steady case in which the wake doublet values are constant along streamline directions and vary only in the spanwise direction. The doublet value for each column of

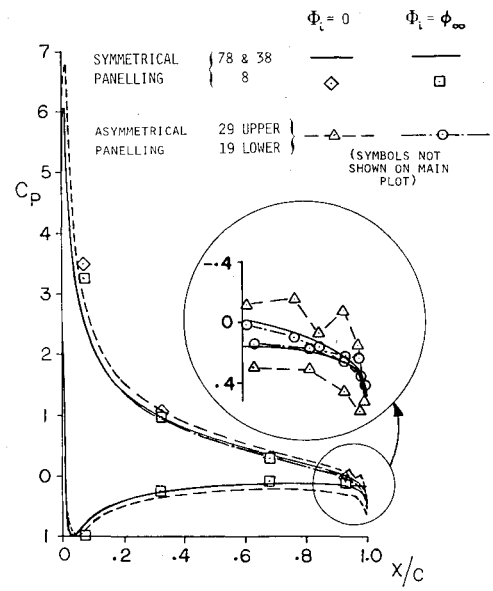

Fig. 3 Calculated pressure distributions on a NACA 0012 section at $\alpha=10$ deg. Comparison of two internal Dirichlet boundary conditions.

Table 1 Calculated lift and drag coefficients for NACA 0012 at 10 deg incidence. Comparison of two internal Dirichlet boundary conditions. Piecewise constant singularity model.[a]

No. of panels	$\Phi_i=0$ C_{L_Γ}	$\Phi_i=0$ C_L	$\Phi_i=0$ C_D	$\Phi_i=\phi_\infty$ C_{L_Γ}	$\Phi_i=\phi_\infty$ C_L	$\Phi_i=\phi_\infty$ C_D
78	1.1947	1.1999	−0.0000	1.1829	1.1866	0.0004
38	1.1814	1.2026	0.0015	1.1607	1.1758	0.0032
8	1.1149	1.2599	0.0926	1.0680	1.1758	0.0892
19+29	1.419	1.428	0.0013	1.1292	1.1323	0.0019

[a] $C_{L_\Gamma}=2\Gamma/V_\infty c$; C_L and C_D from pressure integration.

wake panels is, therefore, determined by the Kutta condition at the trailing edge. From Eq. (3) we simply take the value of $\Phi_U - \Phi_L$ resulting from the surface distribution at each spanwise station. This is the zero load condition. It is not necessary to equate the upper and lower vorticity levels (i.e., doublet gradients)—at least for the simple cases considered here (such an explicit Kutta condition is necessary when modeling large regimes of separated flow[11]). Further, with the piecewise constant singularity model it appears to be unnecessary to extrapolate Φ to the trailing edge to obtain the wake potential jump; the values on the panels adjacent to the trailing edge can be used. (This is an indication that the condition of equal doublet gradients on the upper and lower surfaces is being satisfied by the solution.)

Thus the doublet value on each column of wake panels is

$$\mu_W = \mu_{NU} - \mu_{NL}$$

where *NU, NL* refer to the upper and lower surface panels, respectively, at the start of the column.

The solution of Eq. (5) gives the surface doublet values. A local second-order distribution is then assumed using doublet values located at five panel centers (i.e., a central panel and its four immediate neighbors). The local tangential velocity is then obtained by differentiation. Actually, because we can evaluate the tangential component of the onset flow directly, only the gradient of the *perturbation* component is evaluated in this way; i.e.,

$$V = -\nabla\Phi \qquad \text{or} \qquad V = -\nabla(\mu - \phi_\infty) + V_\infty$$

A number of calculations have been performed using this simple model. (This formulation for the lifting case is in fact simpler than the corresponding source method for the zero-lift case.) Figure 3 shows the results from a two-dimensional case for a NACA 0012 section at 10 deg incidence.

The solid line represents two solutions using 38 and 78 panels in a symmetrical distribution (equal upper and lower). The results are essentially converged using 38 panels. Even an eight-panel case gives a remarkably good solution. These results represent a marked improvement over those obtained on thick wings using the earlier quadrilateral vortex codes (e.g., Ref. 17), based on external Neumann boundary conditions. With that boundary condition special treatment was required near the trailing edge to overcome ill-conditioning caused by the close proximity of the upper and lower doublet sheets. The equivalent internal Dirichlet boundary condition, $\Phi_i = 0$, used here clearly has no such problem when the upper and lower panels are matched. However, a case with an *unequal* number of panels between lower and upper surfaces, i.e., 19 and 29, respectively, had severe mismatching of panels, especially near the trailing edge, and this gave a poor behavior in the pressure distribution—see the enlarged detail in Fig. 3. Also, the circulation level was affected, see Table 1.

An alternative form for the internal flow was therefore considered.

Internal Flow Equal to Onset Flow

The internal Dirichlet condition $\Phi_i = \phi_\infty$ was used earlier by Johnson[8] and also by Bristow[9] but in higher-order formulations. In the present case with $\Phi_i = \phi_\infty$, we set $\Phi_p = \phi_\infty$ in Eq. (2), which now becomes

$$0 = \int\int_{S\text{-}P} \phi \boldsymbol{n}\cdot\nabla\left(\frac{1}{r}\right)\mathrm{d}S - 2\pi\phi_p + \int\int_W (\phi_U - \phi_L)\boldsymbol{n}\cdot\nabla\left(\frac{1}{r}\right)\mathrm{d}W + \int\int_S \frac{1}{r}\boldsymbol{n}\cdot(\nabla\phi_\infty - \nabla\Phi)\,\mathrm{d}S \qquad (6)$$

where ϕ is the perturbation potential on the exterior surface; i.e., $\phi = \Phi - \phi_\infty$.

The source distribution, Eq. (4), now has an additional term,

$$\sigma = V_N + \boldsymbol{n}\cdot V_S - \boldsymbol{n}\cdot V_\infty \qquad (7)$$

For the steady case with a solid boundary, the source term reduces to $\sigma = -\boldsymbol{n}\cdot V_\infty$ in this case. Equation (5) then becomes

$$\sum_{K=1,K\neq J}^{N_S}(\mu_K C_{JK}) - 2\pi\mu_J + \sum_{K=1}^{N_W}(\mu_{W_K} C_{JK}) + \sum_{K=1}^{N_S}\sigma_K B_{JK} = 0 \qquad J = 1, N_S \qquad (8)$$

where B_{JK} is the perturbation potential at the Jth control point due to a unit uniform source distribution on panel K.

Clearly, the source contribution can be evaluated directly and so we have N_S equations in N_S unknown doublet values as before.

Applying this second formulation to the NACA 0012 case in Fig. 3, the solutions for 38 and 78 panels are essentially the same as for the $\Phi_i = 0$ case. There are small differences in the integrated values for C_L, C_D (see Table 1). The case with only eight panels shows a small improvement in the pressure distribution (Fig. 3).

The main point of this calculation with $\Phi_i = \Phi_\infty$ is that with the 19+29 unmatched paneling case, the trailing-edge solution is only affected by a small amount and the circulation value (Table 1) has changed by only 5% from a matched panel case.

Although the unmatched panel case used here represents extremely bad paneling practice—several lower control points are positioned opposite panel corner points on the upper surface—the superior performance of the $\Phi_i = \phi_\infty$ formulation is clearly a very attractive feature to have in a general method.

It will be observed that the second formulation, Eq. (8), is identical to that given by Morino,[10] who used a direct ap-

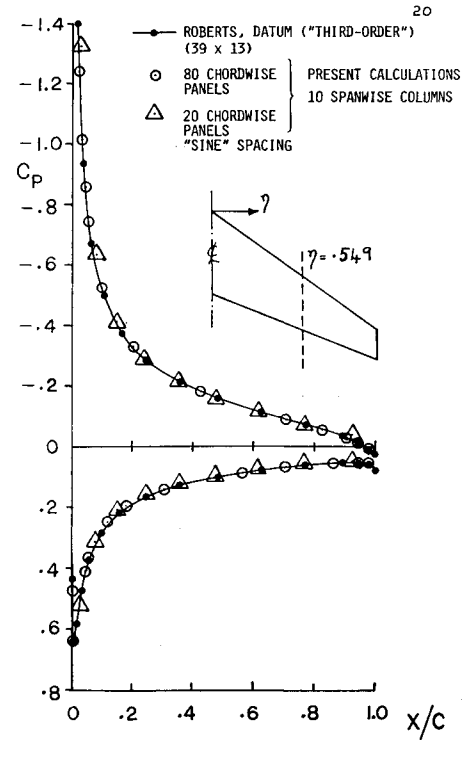

Fig. 4 Comparison of calculated chordwise pressure distributions on a thin swept wing. NACA 0002 section; $\alpha = 5$ deg.

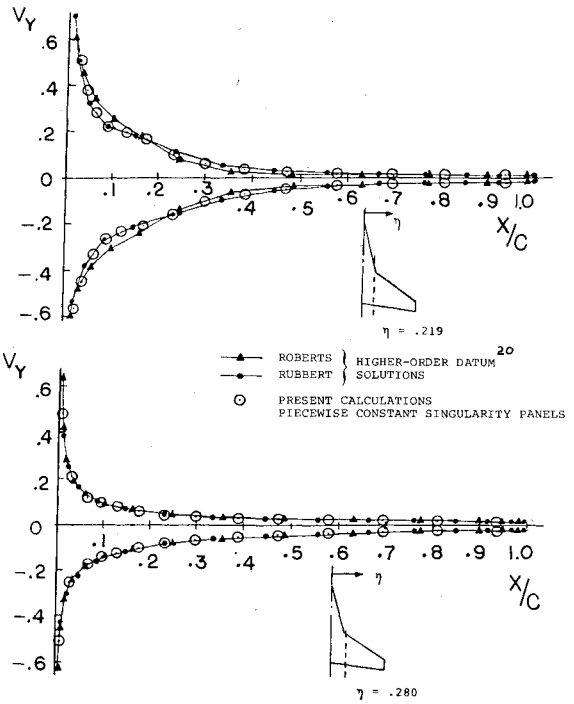

Fig. 5 Comparison of calculated y component of velocity at two stations on a wing with strake. NACA 0002 section; $\alpha = 5$ deg.

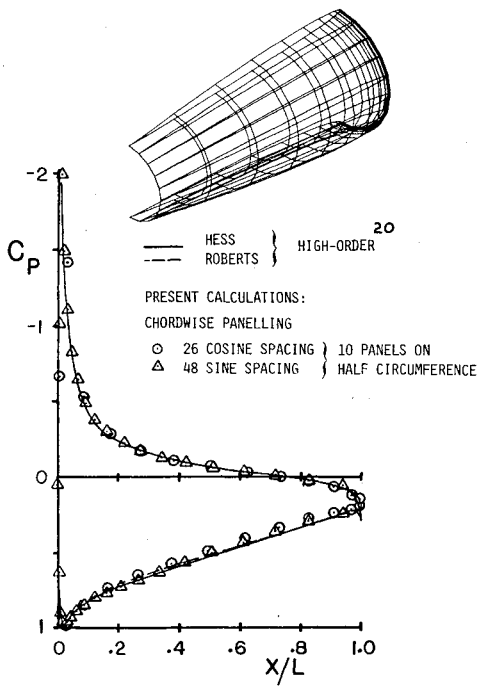

Fig. 6 Comparison of calculated pressure distributions on a nacelle with exit diameter/chord = 0.3. NACA 0005 section; $\alpha = 0$ deg.

plication of Green's Theorem to the external flowfield. Clearly, therefore, Morino's formulation *implies* the condition that the perturbation potential is zero inside the body. The present approach to the formulation based on two regions is easily extended to the case of several regions; this allows a wider range of problems to be considered, of which separated flow modeling[11] is one example.

Discussion of Results

The first three examples discussed below are test cases used in Ref. 20 to compare various panel methods.

For the present calculations the $\Phi_i = 0$ formulation is used in the first example, while in all the other cases the $\Phi_i = \phi_\infty$ form is used. All the examples except the wing-body case are at zero Mach number. In the wing-body case, the Göthert rule transformation is applied.

Swept Wing

Figure 4 shows the chordwise pressure distribution at $\eta = 0.549$ on a thin swept wing at 5 deg incidence. The wing had a midchord sweep of 30 deg, aspect ratio 6, taper ratio ⅓, and a NACA 0012 section. The datum solution[20] for the case is by Roberts' third-order method using a 39 (chordwise) by 13 (spanwise) set of panels. The present calculations were run using 10 spanwise and 80 and 20 chordwise panels on a "cosine" spacing, giving increased panel density towards leading and trailing edges. Roberts' datum paneling is heavily weighted towards the leading edge; there are, in fact, four panels ahead of the most forward panels in the 80 cosine spacing case. (This emphasizes the statements made earlier concerning control point density.)

The characteristics observed in Fig. 1 are seen here also; viz., where the control point density is the same, the low- and high-order solutions are essentially the same. The present calculations using 20 panels deviate from the datum solution near the leading and trailing edges where the control point densities are different. Good agreement is restored in those regions by the 80-panel case, which, at the trailing edge at least, has a similar panel density to the datum case. (Note: Not all the 80-panel pressure values are plotted in the central region of the chord.)

Wing with Strake

The fact that surface velocities are obtained by numerical differentiation in the present method might lead to inaccuracies in awkward situations. So far, no trouble has been experienced. One situation that could be difficult and which has caused a problem for other methods is the evaluation of the spanwise velocity component Vy in the neighborhood of the kink on a wing with strake. In the case considered in Ref. 20, the leading-edge kink occurs at 25% of the semispan and the leading-edge sweep is 75 deg inboard and 35 deg outboard. The trailing-edge sweep is 9 deg. Again the wing section is a NACA 0002 and incidence is 5 deg.

The chordwise distribution of Vy is plotted in Fig. 5 at stations $\eta = 0.219$ and 0.280; i.e., just inboard and just outboard of the kink, respectively.

Two higher-order datum solutions are plotted[20] from Roberts' third-order method and from Johnson and Rubbert's second-order method. These datum solutions agree on the outboard distribution but disagree by a small amount on the inboard cut. The disagreement might be caused by the different ways the interpolation is set up across the kink; i.e., this could be a case of the higher-order assumption "flavoring" the solution as mentioned previously.

The present calculations are in close agreement with the datum solutions and favor the second-order solution near the leading part of the inboard cut. The case was run as part of a "shakedown" exercise of the code and used 946 panels in a 44 (chordwise) by 20 (spanwise) array with 66 panels on the tip-edge surface. The chordwise paneling was on a "sine" distribution with density increasing towards the leading edge. Such a high number of panels was probably not needed for this case, but the calculation took less than 10 min on a CDC Cyber 175 (approximately 2.5 min on a CDC 7600). Including input/output, the total cost of such a run would be about $180 on an overnight priority on a commercial computer.

Nacelle

In the past, low-order solutions for internal flows have suffered badly from "leakage" problems in between control points. The present code was, therefore, applied to the nacelle case considered in Ref. 20. This is an open nacelle with an exit

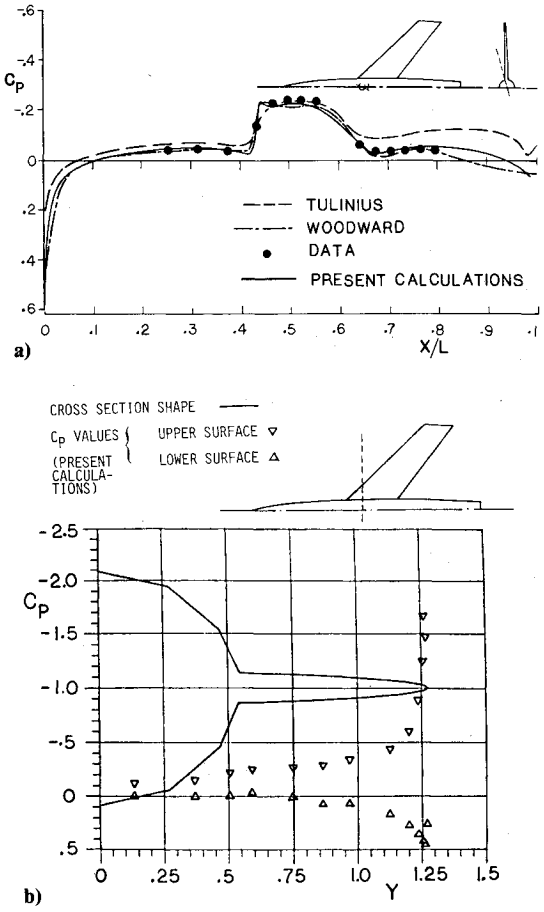

Fig. 7 Pressure distributions on a wing-body configuration at $\alpha = 4$ deg, $M_\infty = 0.6$. a) Above wing-body junction pressures. b) Spanwise cut through present calculations at $X/L = 0.48$.

diameter 0.3 of the chord. The nacelle surface is generated by a NACA 0005 section tilted leading edge out by 5 deg from the x axis.

Two higher-order datum solutions[20] are shown in Fig. 6 for the chordwise pressure distribution. These are due to Hess and also Roberts.

Roberts' solution shows a slightly lower pressure inside the duct compared with Hess' solution. The present calculations were performed using ten panel intervals around half the circumference and with two chordwise distributions, 26 cosine and 48 sine, around the complete section. Both results are in very close agreement with the datum solutions with a tendency for slightly lower pressure inside the duct compared with Hess' solution. This could be caused by the slightly smaller duct cross-section area generated by the present ten *flat* panel representation. Evidently there is no leakage problem with this formulation.

The low panel density case with a total of 260 panels (plus the image set for symmetry) took 52 seconds on a CDC Cyber 175 at a cost of $10 on a weekend priority.

Wing Body

Concave corners have posed a problem to some low-order methods in the past, making it necessary to use high panel densities. Also, such a region might cause a numerical differentiation scheme to misbehave. A wing-body case was, therefore, examined. Figure 7a shows a longitudinal cut through a pressure distribution presented in Ref. 16 for $\alpha = 4$ deg. The cut passes just above the wing-body junction. The present calculations are compared with other solutions and are in good agreement with experimental results.

A spanwise cut through the present calculations at $X/L = 0.48$ is shown in Fig. 7b together with the surface geometry shape. The pressure distribution passes smoothly from the body surface onto the wing surface even though relatively large panels are present on the fuselage side (only six around the half section).

In this calculation the wing and body form one complete volume in which $\Phi_i = \phi_\infty$.

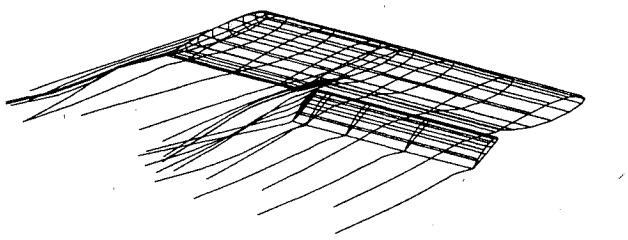

Fig. 8 Calculated wake lines for an aspect ratio 6 wing with part-span Fowler flap.

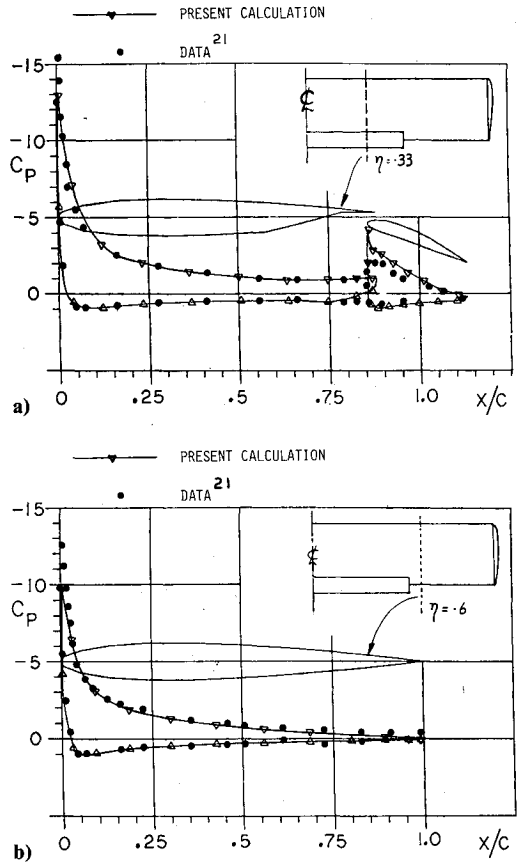

Fig. 9 Comparison of pressure distributions on an aspect ratio 6 wing with part-span Fowler flap; $\alpha = 16$ deg. a) section at $\eta = 0.33$. b) section at $\eta = 0.6$.

Wing Flap

The simple model makes it easy to specify wake shedding virtually anywhere on the surface. Examples of vortex shedding along the tip edge of thick wings were presented in Ref. 13. These calculations used an iterative cycle to relax the wake lines into calculated streamline directions. This calculation has been extended to the case of a wing with part-span flap. Figure 8 shows a general view of a wing-flap configuration at 16 deg incidence. The wake shape is shown after one iteration cycle. The wing has an aspect ratio of 6 and the basic section is a NACA 0012. The 30% chord Fowler flap is deflected 30 deg and the flap cutout extends to $\eta = 0.59$ on the semispan. The surfaces of the wing-tip edge, the flap edge, and the end of the cove are covered with panels.

Vortex separations were prescribed along the wing-tip edge and the flap edge. The present calculations of surface

pressures are compared with experimental data[21] at two stations in Fig. 9. A section through the flap at $\eta = 0.33$ is shown in Fig. 9a and one just outboard of the flap edge at $\eta = 0.6$ in Fig. 9b.

Boundary-layer calculations have not been included in this calculation yet, and so the agreement between the results at this incidence (16 deg) is probably too close. The lower peak suction in the flap data, Fig. 9a, may be caused by interference from a flap support wake.

Conclusions

A piecewise constant singularity panel method based on internal Dirichlet boundary conditions has produced results of comparable accuracy to those from higher-order methods given the same density of control points. Problems associated with earlier low-order panel methods do not appear with this formulation. The method appears to be forgiving when faced with bad panel relationships, provided the zero internal perturbation potential formulation is used. The low computing cost of the method makes it practical for applications to nonlinear problems requiring iterative solutions.

Acknowledgments

Examples shown in this paper are taken from investigations performed under NASA Contracts NAS1-15495, NAS2-8788, and also under Contract N00014-78-C-0128 from the Office of Naval Research.

References

[1] Dvorak, F.A., Maskew, B., and Woodward, F.A., "Investigation of Three-Dimensional Flow Separation on Fuselage Configurations," U.S. Army AMRDL Rept. TR-77-4, March 1977.

[2] Dvorak, F.A., Woodward, F.A., and Maskew, B., "A Three-Dimensional Viscous/Potential Flow Interaction Analysis Method for Multi-Element Wings," NASA CR-152012, July 1977.

[3] Rao, B.M., Maskew, B., and Dvorak, F.A., "Prediction of Aerodynamic Characteristics of Fighter Wings at High Lift," ONR Rept. CR-215-258-1, July 1979.

[4] Woodward, F.A., "USSAERO Computer Program Development, Versions B and C," NASA CR-3227, May 1980.

[5] Piers, W.J. and Slooff, J.W., "Calculation of Transonic Flow by Means of a Shock-Capturing Field Panel Method," *Proceedings of the AIAA Computational Fluid Dynamics Conference,* Williamsburg, Va., July 1979, pp. 147-156.

[6] Roberts, A. and Rundle, K., "Computation of Incompressible Flow about Bodies and Thick Wings using the Spline Mode System," BAC (CAD) Rept. MA19, 1972.

[7] Hess, J.L. and Martin, R.P. Jr., "Improved Solution for Potential Flow about Arbitrary Axisymmetric Bodies by the Use of a Higher-Order Surface Source Method," NASA CR-134694, July 1974.

[8] Johnson, F.T. and Rubbert, P.E., "Advanced Panel-Type Influence Coefficient Methods Applied to Subsonic Flows," *Proceedings of the AIAA 13th Aerospace Sciences Meeting,* Jan. 1975.

[9] Bristow, D.R. and Grose, G.G., "Modification of the Douglas Neumann Program to Improve the Efficiency of Predicting Component Interference and High Lift Characteristics," NASA CR-3020, 1978.

[10] Morino, L., Chen, L.-T., and Suci, E.O., "Steady and Oscillatory Subsonic Aerodynamics around Complex Configurations," *AIAA Journal,* Vol. 13, No. 3, March 1975, pp. 368-374.

[11] Maskew, B., Rao, B.M., and Dvorak, F.A., "Prediction of Aerodynamic Characteristics for Wings with Extensive Separations," Paper No. 31 in *Computation of Viscous-Inviscid Interactions,* AGARD-CP-291, Feb. 1981.

[12] Summa, J.M., "Potential Flow about Three-Dimensional Streamlined Lifting Configurations with Application to Wings and Rotors," Air Force Office of Scientific Research, TR-75-1914, Sept. 1914.

[13] Maskew, B., "Influence of Rotor Blade Tip Shape on Tip Vortex Shedding—An Unsteady Inviscid Analysis," *Proceedings of the 36th Annual Forum of the American Helicopter Society,* Paper 80-6, May 1980.

[14] Maskew, B., "Calculation of Two-Dimensional Vortex/Surface Interference using Panel Methods," NASA CR-159334, Nov. 1980.

[15] Maskew, B., "A Three-Dimensional Viscous/Potential Flow Interaction Analysis Method for Multi-Element Wings; Modification to the Potential Flow Code to Allow Part-Span, High-Lift Devices and Close-Interference Calculations," NASA CR-152227, March 1979.

[16] "Vortex-Lattice Utilization," NASA SP-405, May 1980.

[17] Maskew, B., "Calculation of the Three-Dimensional Potential Flow Around Lifting Non-Planar Wings and Wing-Bodies Using a Surface Distribution of Quadrilateral Vortex Rings," Loughborough University of Technology Rept. TT 7009, 1970.

[18] Jacob, K. and Riegels, F.W., "The Calculation of the Pressure Distribution over Aerofoil Sections of Finite Thickness and without Flaps and Slats," *Zeitschrift fur Flugwissenshaften,* Vol. 11, Part 9, 1963, p. 357-367 [translated as R.A.E. Library Translation No. 1101 (1965)].

[19] Maskew, B., "A Surface Vorticity Method for Calculating the Pressure Distribution over Aerofoils of Arbitrary Thickness and Camber in Two-Dimensional Potential Flow," Loughborough University of Technology Rept. TT 6907, 1969.

[20] Sytsma, H.S., Hewitt, B.L., and Rubbert, P.E., "A Comparison of Panel Methods for Subsonic Flow Computation," AGARD-AG-241, 1979.

[21] Weston, B., "Refinement of a Method for Determining the Induced and Profile Drag of a Finite Wing from Detailed Wake Measurements," Ph.D. Dissertation, University of Florida, March 1981. Also, data to be published in a NASA TP.